Bioactive Materials 9 (2022) 541–553

Contents lists available at ScienceDirect

Bioactive Materials

journal homepage: www.sciencedirect.com/journal/bioactive-materials

Secretions from hypochlorous acid-treated tumor cells delivered in a melittin hydrogel potentiate cancer immunotherapy

Yuhan Zhou [a,1], Ting Ye [a,1], Chengzhi Ye [b,1], Chao Wan [a], Siyue Yuan [a], Yushuai Liu [c], Tianyu Li [a], Fagang Jiang [c], Jonathan F. Lovell [d], Honglin Jin [a,e,*], Jing Chen [a,*]

[a] Cancer Center, Union Hospital, Tongji Medical College, Huazhong University of Science and Technology, Wuhan, 430022, PR China
[b] Department of Pediatrics, Renmin Hospital of Wuhan University, Wuhan, 430060, PR China
[c] Department of Ophthalmology, Union Hospital, Tongji Medical College, Huazhong University of Science and Technology, Wuhan, 430022, PR China
[d] Department of Biomedical Engineering, University at Buffalo, State University of New York. Buffalo, New York, 14260, USA
[e] College of Biomedicine and Health and College of Life Science and Technology, Huazhong Agricultural University, Wuhan, 430070, China

ARTICLE INFO

Keywords:
Cancer immunotherapy
Hydrogel
Melittin
Anti-PD-1
Cell-derived secretions

ABSTRACT

Autologous tumor cells and cell-derived secretions (CDS) can induce antitumor immune responses. The conditions in which cells are cultured and treated impact CDS, and cellular insults alter their composition and function. In this study, we generated CDS from tumor cells exposed to normal culture conditions, hypoxia, cisplatin, radiotherapy, photodynamic therapy, or hypochlorous acid (HOCl). *In vitro* HOCl-CDS showed the strongest stimulatory effects on dendritic cells and macrophages compared to CDS generated by hypoxia, cisplatin, radiotherapy or photodynamic therapy. To improve HOCl-CDS activity at the tumor site, we loaded HOCl-CDS into a melittin-encapsulated hydrogel scaffold. When injected intratumorally, the HOCl-CDS hydrogel promoted tumor cell death, cytotoxic T lymphocyte infiltration, and tumor-associated macrophage reprogramming towards an M1 phenotype. The hydrogel inhibited tumor growth and prolonged the survival of mice bearing B16–F10 melanoma. Furthermore, hydrogel-delivered HOCl-CDS augmented the antitumor effects of immune checkpoint blockade. These results underscore the importance of the CDS generation method and delivery approach for improving cancer immunotherapy.

1. Introduction

Immunotherapy has emerged as a promising cancer treatment strategy, which induces immune responses against cancer cells [1,2]. Immune checkpoint blockade therapies, especially those targeting PD-1, have proved effective in numerous solid malignancies [3,4]. Studies have shown that the high abundance of T cells in the tumor microenvironment (TME) is a key predictor for good response to anti-PD-1. The exhaustion or low frequency of T cells limits the therapeutic effects of cancer immunotherapies [5,6]. According to the cancer-immunity cycle, T lymphocytes are activated by the costimulatory signals of tumor antigens and antigen presenting cells (APCs), migrate to the tumor site, interact directly with cancer cells, and play a powerful tumor killing effect [7]. Therefore, the antitumor function of T cells is highly dependent on two key factors: first, T cells are activated after receiving stimulation signals; second, T cells migrate and infiltrate to the tumor site.

Dendritic cells (DCs), as the most important APCs, are critical for cross-presenting tumor antigens and providing co-stimulatory signals to T cells [8,9]. It has been suggested that DCs are essential for the activation of tumor-specific T cells during anti-PD-1 therapy [10]. Mice depleted for DCs failed to reject tumors in response to anti-PD-1 treatment [10]. Mounting evidence suggests that tumor-associated macrophages (TAMs) are pivotal for the migration of $CD8^+$ T cells in the TME [11]. TAMs are commonly induced by tumor cells to differentiate towards suppressive M2-like TAMs, which impair the motility of $CD8^+$ T cells and limit T cells migration into tumor site [11,12]. Importantly, macrophages depletion enhanced $CD8^+$ T cell recruitment in the TME and augmented the therapeutic effect of anti-PD-1 [11,13]. TAMs also promote resistance to anti-PD-1/PD-L1 antibodies independently. PD-1^-

Peer review under responsibility of KeAi Communications Co., Ltd.

* Corresponding authors. Cancer Center, Union Hospital, Tongji Medical College, Huazhong University of Science and Technology, Wuhan, 430022, PR China.
E-mail addresses: jin@hust.edu.cn (H. Jin), chenjingwh@hust.edu.cn (J. Chen).

[1] These authors contributed equally to this work.

https://doi.org/10.1016/j.bioactmat.2021.07.019
Received 12 April 2021; Received in revised form 1 July 2021; Accepted 18 July 2021
Available online 24 July 2021

macrophages seize anti-PD-1 and interfere with anti-PD-1 binding to the surface of T cells, hampering the reactivation of exhausted T cells [14]. Moreover, TAMs enhance tumor progression by promoting cancer stem cell development, angiogenesis epithelial to mesenchymal transition, and metastasis [12,15]. Thus, developing strategies to activate DCs and inhibit M2-TAMs is essential to maximize T cell activation and infiltration upon immunotherapy.

Chemotherapy, radiotherapy, oncolytic viruses, and intratumoral delivery of immunomodulatory agents are known to reshape the TME [16,17]. Autologous tumor cell-derived secretions (CDS) have attracted interest, as they have minimal side effects and are inherently personalized cancer treatments. CDS can deliver tumor antigens to DCs and induce $CD8^+$ T cell-dependent antitumor responses *in vivo* [18]. A phase I clinical trial has shown that CDS containing MAGE3 peptides activated immune responses in melanoma patients [19]. So far, most studies have focused on exosomes or microparticles in tumor cell-derived secretions, sometimes from cells provided exogenous treatments. During cancer progression, cell secretions produced under physiological conditions may have properties to suppress immune responses and promote metastasis [20,21]. However, under certain conditions, such as exposure to radiation, heat, or ultraviolet light, exogenously treated tumor cells can release extracellular vesicles with immunostimulatory properties [22–25]. UV-exposed tumor-derived microparticles (UV-TMPs) promoted DC maturation and activated antitumor T cell immunity [22,25]. Nevertheless, UV-TMPs from lung cancer cells induced M2-macrophages polarization and promoted tumor progression [26,27], suggesting that the conditions in which cells are cultured and treated influence CDS composition and function. The ideal CDS preparation conditions to maximize their immunostimulatory effects is largely unknown. Furthermore, as secretions are quickly absorbed and degraded in the body, and themselves often lack or have weak direct tumor cell killing function, the development of suitable CDS delivery platforms that ensure sustained and direct antitumor effects for the case of intratumoral administration is also required [28,29].

In this study, we assessed effects of hypoxia, cisplatin (DDP), radiotherapy (RAD), photodynamic (PDT) and hypochlorous acid (HOCl) treatments on CDS. We found that HOCl-treated tumor CDS (HOCl-CDS) significantly promoted DC maturation and macrophage polarization towards an M1 phenotype, leading to potent immunostimulatory effects. To enhance the direct cytotoxic effects and prolong the retention of HOCl-CDS in the TME, we employed a synthetic peptide hydrogel, wherein melittin (MEL) was linked to the polypeptide $RADA_{24}$ by physical cross-linking methods to obtain a fusion MELR hydrogel [30]. This MELR hydrogel showed superior drug loading capacity, sustained drug release, and cytotoxic effects. HOCl-CDS loading in the MELR hydrogel achieved 100 % entrapment efficiency and formed a multifunctional HOCl-CDS hydrogel. HOCl-CDS hydrogel administration promoted direct tumor cell death and immune remodeling of the TME, leading to antitumor efficacy against subcutaneous melanoma *in vivo* in mice. Further, the combination of immune stimulation and tumor cell killing provided by the HOCl-CDS hydrogel augmented antitumor effects of anti-PD-1 treatment.

2. Materials and methods

2.1. Materials

$RADA_{24}$-melittin fusion peptide (Ac-RADARADARADARADAR-ADARADA-GG-GIGAVLKVLTTGLPALISWIKRKRQQ-NH_2), and $RADA_{24}$ peptide (Ac-RADARADARADARADARADARADA-NH_2) were synthesized by Bankpeptide Ltd. (Hefei, China). The peptides were stored at −20 °C until use.

2.2. Cells and animals

B16–F10 cells were kindly provided by Professor Zhihong Zhang (HUST, Wuhan, China). Firefly luciferase was stably transfected to B16–F10 cells to establish the B16-LUC cell line. Cells were cultured in RPMI-1640 medium (Gibco) containing 10 % fetal bovine serum (FBS; Gibco) and 1 % antibiotics (penicillin and streptomycin) in a 37 °C and 5 % CO_2 incubator. Female C57BL/6 mice (6 weeks old) were purchased from CTGU Laboratory Animal Center (Yichang, China). All animal procedures were conducted according to the Guide for the Care and Use of Laboratory Animals, and were approved by the Animal Experimentation Ethics Committee of Tongji Medical College, Huazhong University of Science and Technology (Wuhan, China).

2.3. Preparation of CDS

To prepare HOCl-CDS, the NaOCl reagent (China Meklin) was first diluted with Hank's Balanced Salt Solution (HBSS) to prepare 70 μmol/L hypochlorous acid (HOCl) solution; HOCl solution was added to the culture medium of B16–F10 cells that reached a final cell density of 8×10^5/mL. After incubation for 4 h, the cell culture was harvested and centrifuged at 1000×*g* for 10 min and 14,000×*g* for 2 min to remove cellular debris. The supernatant was transferred into a Amicon Ultra-15 Centrifugal Filter Unit (15 mL/3 kDa, Millipore) and centrifuged at 5000×*g* for 20 min. Next, 10 mL ultrapure water or PBS was added and centrifuged to thoroughly remove excess ClO^-. Finally, we obtained 50 μL of HOCL-CDS from 4×10^6 B16–F10 cells for further assays *in vivo*, or obtained 20-fold concentrated HOCl-CDS for further assays *in vitro*. A conventional BCA protein quantitation assay was used to detect the protein concentration. The concentration of serum proteins in the culture media was also measured and was subtracted from the CDS samples to determine CDS protein level. To prepare hypoxia-CDS, we cultured 8×10^5/mL B16–F10 cells at 37 °C, 94 % N_2, 5 % CO_2, and 1 % O_2 for 48 h. The cell culture medium was collected, centrifuged, and ultrafiltrated, as described earlier, with the protein concentration of 0.44 mg/mL. To prepare DDP-CDS, 8×10^5/mL B16–F10 cells were cultured with 40 μmol/L DDP (Sigma, USA) for 48 h; the medium was collected, centrifuged, and ultrafiltrated, with the protein concentration of 0.12 mg/mL. To prepare RAD-CDS, 8×10^5/mL B16–F10 cells were irradiated with a single dose of 20 Gy by 6-MV x-rays (600 MU/min, Trilogy System Linear Accelerator, Varian Medical Systems). After incubation for 72 h, the medium was collected, centrifuged, and ultrafiltrated, with the protein concentration of 0.83 mg/mL. To prepare PDT-CDS, 8×10^5/mL B16–F10 cells were seeded in 6-cm cell culture dishes, incubated with 1 μg/mL Ce6 photosensitizer for 12 h, and irradiated by a 660 nm NIR laser (1.5 W/cm^2) for 1 min. After incubation for 48 h, the medium was collected, centrifuged, and ultrafiltrated, with the protein concentration of 0.82 mg/mL.

2.4. Hydrogel synthesis

MELR peptide (10 mg) was dissolved in 1 mL 0.9 % NaCl solution and kept at 4 °C overnight to form MELR hydrogel. HOCl-CDS hydrogel was formed by dissolving 10 mg MELR peptide in 1 mL mixed solution of 0.9 % NaCl and HOCl-CDS. $RADA_{24}$ hydrogel was prepared in the same way for replacing the MELR peptide by the equal amount of $RADA_{24}$ peptide; the solution was incubated at 4 °C overnight.

2.5. Transmission electron microscopy (TEM) photography of the hydrogel

The morphology and structure of MELR and HOCl-CDS hydrogel were assessed by TEM. The hydrogel was diluted (1:100) with ultrapure water, deposited (10 μL) on the surface of fresh copper grids for 2 min, and negatively stained with phosphotungstic acid (5 %) for 30 s. After air-drying, the hydrogel grids were subjected to TEM (Titan G2 60–300, FEI Company, OR, USA).

2.6. Rheological test

Frequency sweep analysis was performed using 1 % (w/w) HOCl-CDS hydrogel. A constant strain was maintained at 0.1 % to detect the storage modulus (G′) and loss modulus (G″) with continuous frequency (0.1–100 rad/s). The thixotropic analysis was performed using 1 % (w/w) hydrogel at the frequency of 1 rad/s. In the first 200 s, the HOCl-CDS hydrogel was detected under a low strain rate of 0.1 %; between 200 s and 400 s, the gel was kept at a higher strain rate of 40 %. The strain rate was then returned to 0.1 % and to record the restoration process. These analyses were conducted using a rheometer (DHR-2, TA, Instruments, New Castle, DE).

2.7. Cell viability

B16–F10 cells (5000 cells/well in 100 μL) were seeded in 96-well plates and incubated for 24 h. Subsequently, the medium was replaced by 180 μL culture medium and 20 μL PBS, MELR hydrogel, $RADA_{24}$ hydrogel or HOCl-CDS hydrogel. After incubation for 1, 3, 5, and 7 d, cell viability was assessed using a CCK-8 assay kit (BS350B, Biosharp).

2.8. Hemolysis assay

Red blood cells (RBCs), diluted to 5×10^7 cells/mL, from mouse retro-orbital blood were incubated with different concentrations of free melittin, MELR hydrogel, or HOCl-CDS hydrogel at 37 °C for 4 h; PBS buffer and 1 % Triton X-100 treatments served as a negative and positive control, respectively. After centrifugation for 10 min, the optical absorbance of supernatants was detected at 540 nm (Tecan Group Ltd., Mannedorf, Switzerland); the percentage of hemolysis was calculated by the formula: hemolysis rate (%) = [(ODsample-ODnegative)/(ODpositive-ODnegative)] × 100 %.

2.9. Generation and stimulation of bone marrow-derived DCs (BMDCs) and bone marrow-derived macrophages (BMDMs)

BMDCs were isolated from limbs of C57BL/6 mice and cultured in RPMI-1640 medium containing 10 % FBS and 20 ng/mL GM-CSF (PeproTech) to stimulate cell differentiation. BMDCs were harvested on the 7th day for further analyses. BMDMs were isolated from C57BL/6 mice in the same way and cultured in a medium containing 20 ng/mL M-CSF (PeproTech). To induce M2 polarization, we treated BMDMs with 20 ng/mL IL-4 and IL-13 (PeproTech) in the culture on the 5th day. Cells were harvested after 48 h.

2.10. ATP release assay

Extracellular ATP in CDS was detected using an Enhanced ATP Assay Kit (Beyotime). CDS was prepared and transferred to 96-well plate, and ATP concentration was measured following the manufacturer's instructions of Enhanced ATP Assay Kit.

2.11. ELISA assays

For the measurement of HMGB1, TNF-α, IL-1α, GM-CSF, M-CSF, MIP-3α, MIP-1α, ENA78, CD40L, MCP-1, IL-12, IL-2, TGF-β1, PGE2 and IL-6 levels in the various CDS, ELISA assays were conducted using HMGB-1 ELISA Kit (E08225 m, CUSABIO), TNF-α ELISA Kit (E-EL-M0049c, Elabscience), IL-1α ELISA Kit (E-EL-M0036c, Elabscience), GM-CSF ELISA Kit (E-EL-M0032c, Elabscience), M-CSF ELISA Kit (E-EL-M2445c, Elabscience), MIP-3α ELISA Kit (E-EL-M0013c, Elabscience), MIP-1α ELISA Kit (E-EL-M0007c, Elabscience), ENA78 ELISA Kit (SEA860Mu, Cloud-Clone), CD40L ELISA Kit (SEA119Mu, Cloud-Clone), MCP-1 ELISA Kit (E-EL-M3001, Elabscience), IL-12/p70 ELISA Kit (E04600 m, CUSABIO), IL-2 ELISA Kit (E04627 m, CUSABIO), TGF-β1 ELISA Kit (E04726 m, CUSABIO), PGE2 ELISA Kit (E07966 m, CUSABIO) and IL-6 ELISA Kit (E04639 m, CUSABIO) following the manufacturer's instructions.

2.12. Real-time PCR (RT-PCR)

Total RNA from BMDCs was extracted using a MicroElute Total RNA Kit R6831-01 (OMEGA), cDNA was synthesized using a HiScript III RT SuperMix for qPCR (+gDNA wiper; Vazyme). Reactions were prepared using AceQ Universal SYBR qPCR Master Mix (Vazyme) and were run on a StepOnePlus Real-Time PCR System (Thermo Fisher Scientific). The mRNA levels of target genes were normalized to those of *GAPDH*. The primer sequences were as follows: *IFN-α* (ATGACCTGCAAGGCTGTCTG, AGACTTCTGCTCTGACCACCTC), *IFN-β* (CAGCTCCAAGAAAGGACGAAC, GGCAGTGTAACTCTTCTGCAT), and *IL-6* (TTGGGACTGATGCTGGTGAC, GTGGTATAGACAGGTCTGTTGGG). All primers were synthesized by GeneCreate Biological Engineering Co. Ltd. (Wuhan).

2.13. Western blotting

BMDCs treated with PBS or HOCl-CDS hydrogel for 2 h were lysed by RIPA buffer with protease inhibitors and phosphatase inhibitor cocktails A and B on ice for 30 min. The cell lysate was centrifuged at 12,000 rpm for 30 min, and the protein supernatant was harvested, boiled at 100 °C for 10 min, and stored at −20 °C for further use. Proteins were separated by 10 % SDS-polyacrylamide gel, transferred to PVDF membranes, blocked by 5 % skim milk powder for 1 h at room temperature, and then incubated overnight at 4 °C with specific anti-p-TBK1 (D52C2, Cell Signaling Technology, 1:200), TBK1 (#3013, Cell Signaling Technology, 1:500), p-IRF3 (D601 M, Cell Signaling Technology, 1:200), IRF3 (D83B9, Cell Signaling Technology, 1:500). Membranes were washed the next day, incubated with secondary antibody at room temperature for 1 h, and finally visualized by NcmECL Ultra (NCM Biotech).

2.14. Animal models and treatments

To establish melanoma tumors in mice, B16–F10 cells (5×10^5 cells/mouse) were subcutaneously injected into the right flanks of mice. 7 d after inoculation, mice were randomly allocated into different treatment groups and intratumorally injected with 50 μL PBS, MELR hydrogel (1 mg, 50 μL), HOCl-CDS (containing 4×10^6 B16–F10 cells/mouse, 50 μL), or HOCl-CDS hydrogel (containing 1 mg MELR and 4×10^6 B16–F10 cells/mouse, 50 μL). A total of 3 doses were administered every 3 d. For mice treated with HOCl-CDS hydrogel combined with anti-PD-1, 4 doses of anti-PD-1 (100 μg per dose; BE0146, BioXcell) were intraperitoneally administered every 2 d. Tumor growth was monitored every 2 d; tumor volume was calculated as $\text{width}^2 \times \text{length}/2$. Tumor tissues, lymph nodes, and blood were harvested for further analyses. Major organs, including the hearts, livers, spleens, lungs, and kidneys, were harvested for histological analyses.

2.15. Flow cytometry

For DCs analyses, cells were stained for markers CD11c (clone N418), CD80 (clone 16-10A1), and CD86 (clone GL-1). For TAMs analysis, single-cell suspensions from tumor tissues were prepared and stained with CD45 (clone 30-F11), CD11b (clone M1/70), F4/80 (clone BM8), CD86 (clone GL-1), and CD206 (clone C068C2). To assess tumor-infiltrating lymphocytes (TILs), single-cell suspensions were prepared from tumor tissues and treated for 4–6 h with Phorbol 12-myristate 13-acetate (PMA; 100 ng/mL; Abcam), monensin sodium salt (1 μg/mL; Biolegend), ionomycin (100 ng/mL; PeproTech); cells were stained with CD3e (clone 145-2C11), CD4 (clone GK1.5), CD8a (clone 53–6.7), fixed and permeabilized, and then stained with IFN-γ (clone XMG1.2). All flow cytometry antibodies were purchased from Biolegend.

2.16. Bioluminescent imaging

B16-LUC melanoma-bearing mice were anesthetized with 1 % pentobarbital sodium and intraperitoneally injected with 150 mg/kg firefly luciferin (103404-75-7, Thermo Life). After 10 min, luciferase imaging was performed using the Bruker In Vivo MS FX PRO Imager (30 s exposure time). For the release dynamics analyses, ReadLink™ Rapid iFluor™ 750 Antibody Labeling Kits (Catalog number: 1250, AAT Bioquest) were used to conjugate fluorescent dye to HOCl-CDS. 50 μL of iFluor™ 750 Dye loaded HOCl-CDS solution or iFluor™ 750 Dye loaded HOCl-CDS hydrogel were subcutaneously injected into the right flank of C57BL/6 mice, and mice were imaged at different time points (excitation wavelength: 750 nm, emission wavelength: 790 nm).

2.17. Statistical analysis

All data were analyzed using GraphPad Prism 7.0 software. Statistical significance was determined by a two-tailed Student's *t*-test, and mouse survival was assessed by the Kaplan-Meier method. *, $p < 0.05$; **, $p < 0.01$; ***, $p < 0.001$.

3. Results

3.1. Preparation of HOCl-treated tumor CDS to stimulate DCs and macrophages

We exposed B16–F10 cells to hypoxia, DDP, RAD, PDT, or HOCl to obtain the resulting CDS (Fig. 1a). 95 % cell death was set as the criteria to obtain optimum doses or concentrations of these treatments. 70 μM HOCl was used and caused over 95 % cell necrosis (Fig. S1). The effects of the resulting CDS on DCs maturation and macrophages polarization were assessed *in vitro*. BMDCs were treated with CDS from cells provided different treatments for 24 h, and the expression of CD80 and CD86 was analyzed by flow cytometry. We found that the number of mDCs ($CD80^+CD86^+$) induced with HOCl-CDS treatment was 2.6-fold higher than treatment with CDS from PBS treatment. HOCl-CDS-treated DCs exhibited the highest CD80 and CD86 expression levels among all CDS treatment groups (Fig. 1b). The culture supernatants of DCs treated by different types of CDS were collected and profiled with cytokine ELISA assay. The HOCl-CDS treated group displayed the highest level of IL-2 and IL-12, which was consistent with the activation level of DCs (Fig. S2). Additionally, BMDMs treated with HOCl-CDS showed increased CD86 expression and reduced CD206 expression, providing the strongest M1-polarizing effect (Fig. 1c). These results suggested that HOCl treatment was an effective approach to generate immunostimulatory CDS. We assessed damage associated molecular patterns (DAMPs) release by HOCl-treated B16F10 cells (Fig. 1d). Extracellular ATP and HMGB1 levels in HOCl-CDS were 23.4-fold and 2.5-fold of that in the untreated CDS, respectively (Fig. 1e). Moreover, tumor necrosis factor alpha (TNF-α), interleukin 1 alpha (IL-1α), granulocyte-macrophage colony-stimulating factor (GM-CSF), macrophage colony-stimulating factor (M-CSF), macrophage inflammatory protein 3 alpha (MIP-3α), macrophage inflammatory protein 1 alpha (MIP-1α), epithelial-derived neutrophil-activating peptide 78 (ENA78), CD40 ligand (CD40L), monocyte chemoattractant protein 1 (MCP-1), which were involved in DCs maturation and macrophages polarization, were significantly secreted higher in the HOCl-CDS (Fig. 1f).

3.2. Preparation and characterization of HOCl-CDS hydrogel

To achieve sustained release effect of HOCl-CDS, we designed a melittin-$RADA_{24}$ (MELR) hydrogel scaffold. Loading HOCl-CDS into MELR at a final concentration of 0.9 % NaCl (w/w) could form the stable HOCl-CDS hydrogel with nearly 100 % encapsulation efficiency, indicating that MELR was a suitable delivery platform (Fig. 2a). The microscopic morphology and structure of HOCl-CDS and MELR hydrogels were assessed by TEM. MELR and HOCl-CDS hydrogels self-assembled into networks of interwoven nanofibers with diameters of 10.2 ± 2.9 and 11.8 ± 1.2 nm, respectively (Fig. 2b). The viscosity and hardness of HOCl-CDS hydrogels were assessed by rheological analysis. The storage modulus (G′) and loss modulus (G″) were slightly dependent on the angular frequency when the strain rate was maintained at 0.1 %, indicating the stability of the HOCl-CDS hydrogels (Fig. 2c and d). In the time-dependent rheological test, the storage modulus and loss modulus of HOCl-CDS hydrogel were generally stable at a fixed low strain rate of 0.1 % in the first 200 s. At 200 s–400 s, the gel was fragmented at a strain rate of 40 %. When the strain rate was returned to 0.1 %, the hydrogel acquired the original viscosity and hardness, confirming the favorable rheological properties of HOCl-CDS hydrogels.

To assess the release dynamics of HOCl-CDS hydrogels, fluorescent iFluorTM 750 Dye was used to label HOCl-CDS. The Dye-HOCl-CDS solution (Dye) or Dye-HOCl-CDS hydrogel (Dye hydrogel) were subcutaneously injected into the right flank of C57BL/6 mice and the fluorescent release efficiency was assessed. The fluorescence intensity of the Dye-HOCl-CDS group and the Dye-HOCl-CDS hydrogel group within 2 h were similar. At 6 h, the fluorescence in Dye-HOCl-CDS group attenuated, and could hardly be seen, whereas Dye-HOCl-CDS hydrogel group remained relatively high (Fig. 2e and f). At the experimental endpoint (day 7), the fluorescence of Dye-HOCl-CDS hydrogel group could still be slightly observed (Fig. S3). These results indicated that HOCl-CDS encapsulated by MELR hydrogel could have sustained released *in vivo*.

Hemolysis assays were performed to assess whether MELR and HOCl-CDS hydrogels affected red blood cells (RBCs) integrity. Complete hemolysis was observed with 6.4 μM free melittin. MELR hydrogel at 50 μM led to a hemolysis rate of 5.8 %, whereas HOCl-CDS hydrogels had little effect on RBCs integrity (Fig. 2g and h). The reduction of the hemolysis by melittin may be due to the increased size and modified amino acid content which might decrease affinity and binding to erythrocytes after melittin was linked to the polypeptide $RADA_{24}$. The morphology of solid hydrogel likely further weakened the lytic effect [30,31]. These findings suggested that the peptide fusion approach to construct HOCl-CDS hydrogels greatly decreased the hemolytic effect of melittin and that MELR hydrogel was the relatively safe HOCl-CDS delivery platform.

3.3. In vitro immune activation and antitumor effect of HOCl-CDS hydrogel

To evaluate the immune activation effect of HOCl-CDS hydrogel *in vitro*, BMDCs was cultured with PBS, MELR, free HOCl-CDS, HOCl-CDS hydrogel or lipopolysaccharide (LPS) for 24 h, and the expression of CD80 and CD86 was analyzed by flow cytometry. MELR and free HOCl-CDS increased the percentage of $CD80^+CD86^+$ DCs, indicating that they effectively stimulated DCs maturation. The maturation rate in DCs treated with HOCl-CDS hydrogel was 69.5 %; this rate was 2.0-fold of that in PBS group, 1.5-fold of that in MELR hydrogel group, 1.2-fold of that in free HOCl-CDS group, and close to that of lipopolysaccharide (LPS) positive control group (Fig. 3a and b). The mRNA expression levels of IFN-α, IFN-β, and IL-6 in BMDCs were significantly increased in response to HOCl-CDS hydrogel treatment. In addition, increased phosphorylation of TBK1 and IRF3 was observed in BMDCs, suggesting that the HOCl-CDS hydrogel activated the cGAS-STING pathway (Fig. 3c and d). These findings suggested that the HOCl-CDS hydrogel was a potent stimulator of DCs maturation and immune responses. To explore the effects of HOCl-CDS hydrogel on macrophage polarization, IL-4-induced M2-macrophages were cultured with HOCl-CDS hydrogel for 24 h and the expression of CD86 and CD206 was analyzed by flow cytometry. HOCl-CDS hydrogel increased the expression levels of the M1 marker CD86 and reduced the expression levels of the M2 marker CD206, indicating that HOCl-CDS hydrogel promoted reprogramming of M2-macrophages toward M1 phenotype (Fig. 3e and f).

In vitro antitumor effects of HOCl-CDS hydrogel on B16–F10 cells

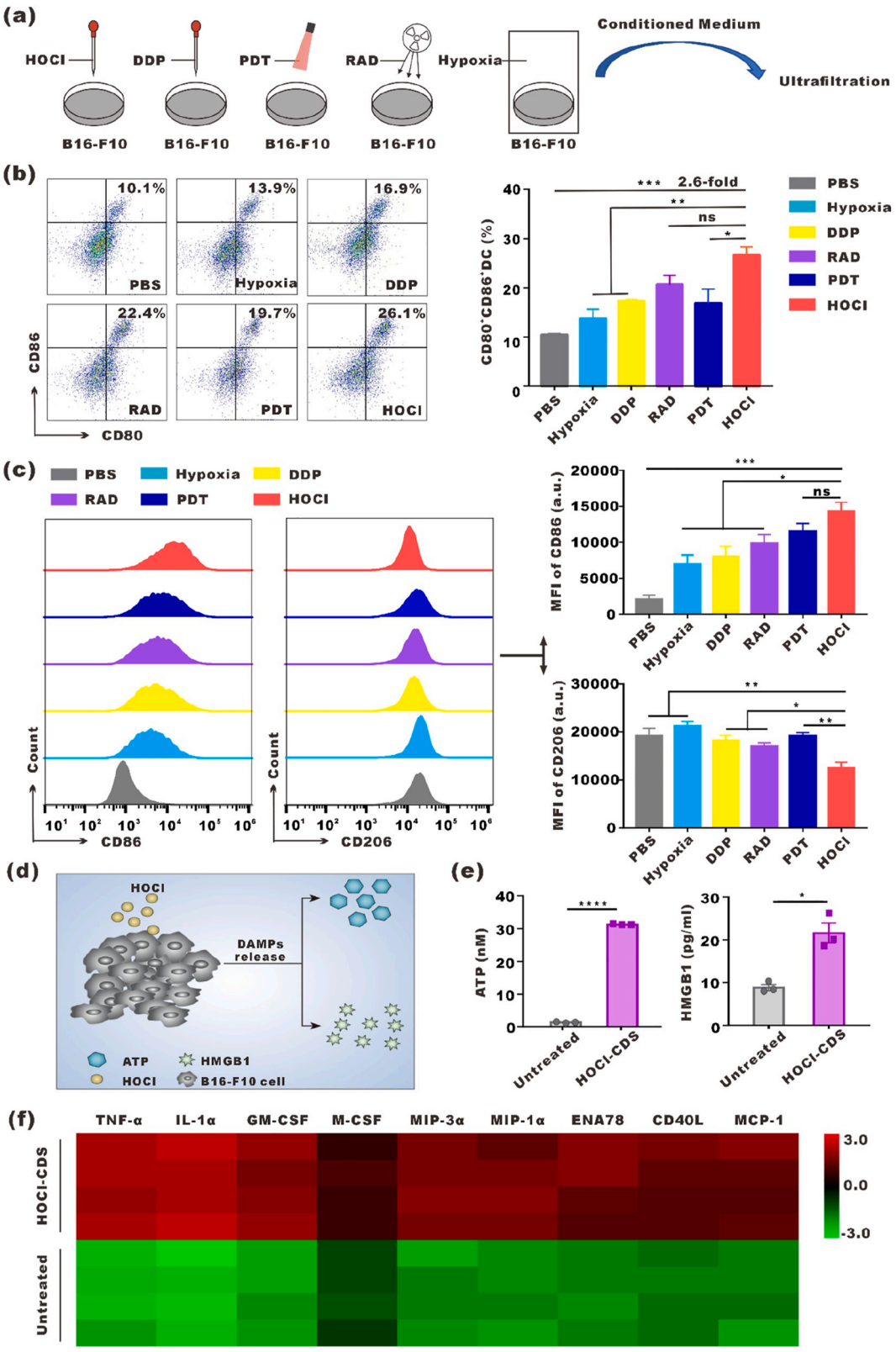

Fig. 1. Preparation of different CDS and their stimulatory effects on DCs and macrophages. **a** Schematic diagram showing 5 different treatments to obtain the corresponding CDS. **b** Flow cytometry analyses of CD80 and CD86 expression on BMDCs stimulated with the different CDS for 24 h. **c** Flow cytometry analyses of CD86 and CD206 expression in BMDMs stimulated with the different CDS for 24 h. **d** Schematic diagram of DAMPs release by HOCl-treated B16F10 cells. **e** Extracellular levels of ATP and HMGB1 in HOCl-CDS and the untreated CDS. **f** Heat map of differentially secreted proteins in HOCl-CDS and the untreated CDS.

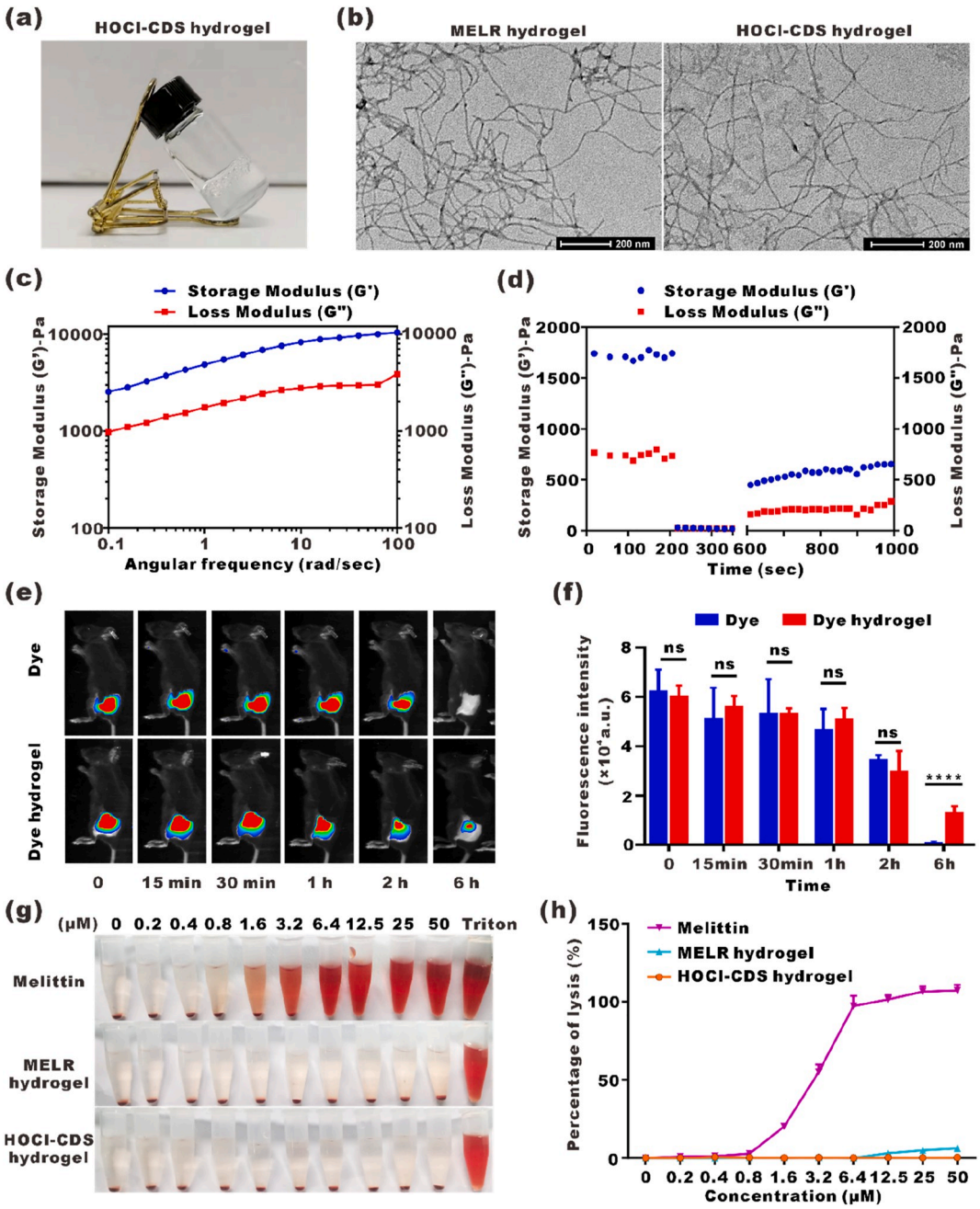

Fig. 2. Preparation and characterization of the HOCl-CDS hydrogel. **a** Photograph of the HOCl-CDS hydrogel. **b** Representative TEM images of MELR and HOCl-CDS hydrogels. **c, d** Frequency sweep rheological analysis and step-strain time-dependent rheological analysis of the HOCl-CDS hydrogel. **e** NIR fluorescence imaging of the Dye hydrogel and free Dye at different time points. **f** Statistic analysis of the fluorescence intensity from **e**. **g** Hemolytic effects of free melittin solution, MELR hydrogel, and HOCl-CDS hydrogel. **h** Hemolysis rate of free melittin solution, MELR hydrogel, and HOCl-CDS hydrogel.

were assessed by CCK-8 assay. MELR, HOCl-CDS hydrogel and $RADA_{24}$ hydrogel were added to B16–F10 cells culture medium. At day 1, 3, 5, and 7, the viability of HOCl-CDS hydrogel-treated cells was 26.1 %, 16.5 %, 13.5 %, and 9.9 %, respectively, whereas that of MELR-treated cells was 15.7 %, 10.5 %, 8.3 %, and 8.5 %. Moreover, $RADA_{24}$ hydrogel did not show any cytotoxicity in the tested concentrations, which indicated that the direct tumor cells killing effects of MELR and HOCl-CDS hydrogel mainly from the antitumor activity of melittin (Fig. 3g). We also treated B16–F10 cells with HOCl-CDS or ultrafiltered HOCl solution (70 μM) for 24 h and found that neither HOCl-CDS nor ultrafiltered HOCl solution caused significant cytotoxicity (Fig. S4). The cytotoxicity of the MELR hydrogel was further assessed in various cell lines including B16–F10 cells, DCs and bEnd.3 cells (brain-derived endothelial cells). The results showed that the killing effect of MELR on DCs was weaker than that in B16–F10 cells and bEnd.3 cells (Fig. S5).

3.4. In vivo antitumor effects of HOCl-CDS hydrogel

To evaluate the therapeutic effect of HOCl-CDS hydrogel on aggressive melanoma, we subcutaneously inoculated B16–F10 cells into C57BL/6J mice. When tumor volume reached 30 mm^3, mice were intratumorally injected with PBS, MELR (1 mg), HOCl-CDS (containing 4×10^6 B16–F10 cells per mouse), or HOCl-CDS hydrogel (containing 1 mg MELR and 4×10^6 B16–F10 cells per mouse) (Fig. 4a). The latter 3 treatments exerted antitumor effects to some extent. Treatment with MELR hydrogel delayed tumor growth in the first week; however, the

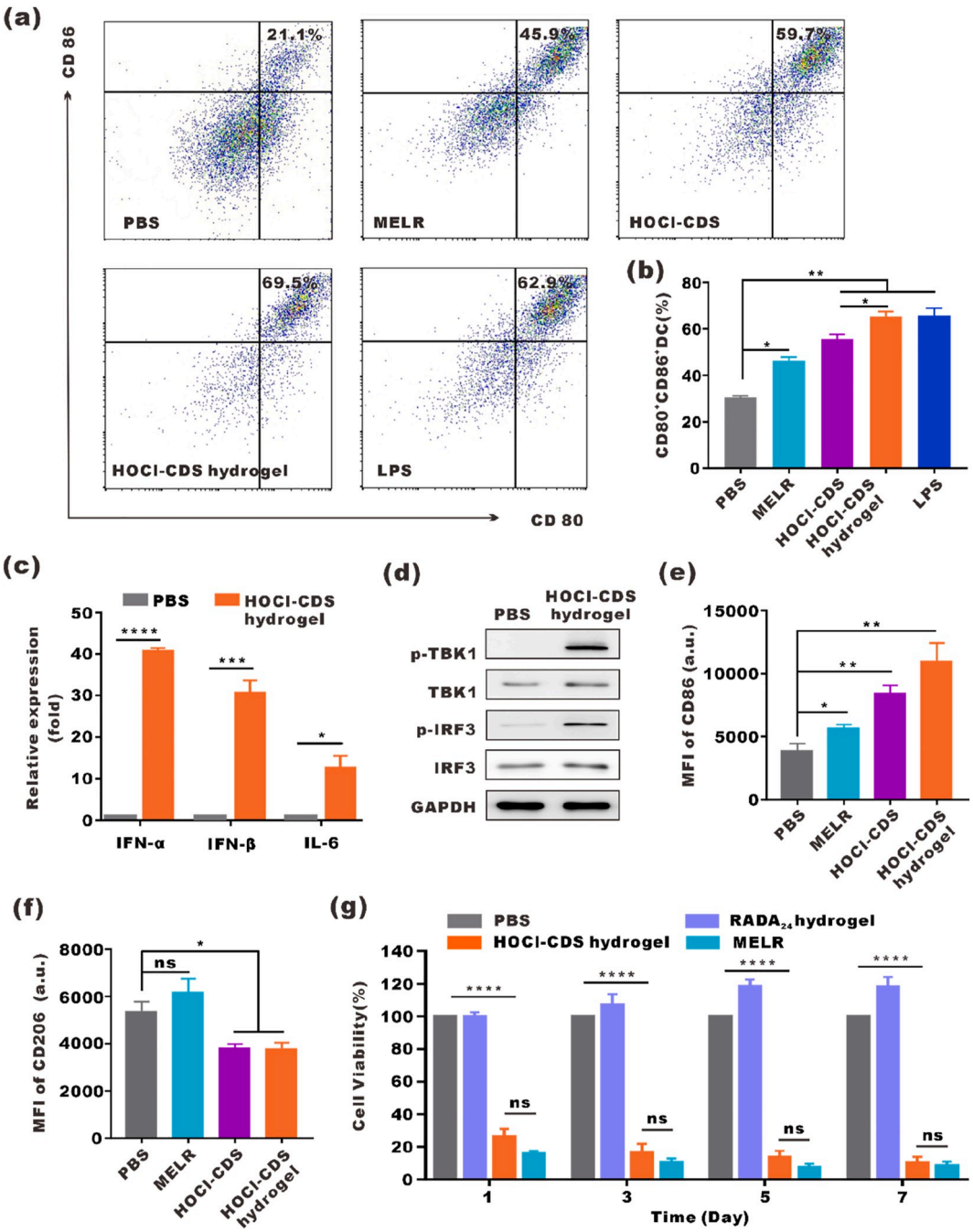

Fig. 3. *In vitro* immune activation and antitumor effect by the HOCl-CDS hydrogel. **a** Flow cytometry analyses of CD80 and CD86 expression on BMDCs treated with PBS, MELR, HOCl-CDS, or HOCl-CDS hydrogel. LPS served as a positive control. **b** Statistical analysis of data from **a**. **c** The mRNA levels of IFNα, IFNβ, and IL-6 in BMDCs treated with HOCl-CDS hydrogel. **d** Western blot showing the expression of p-TBK1, TBK1, p-IRF3, IRF3 in murine BMDCs treated with PBS and HOCl-CDS hydrogel for 2 h. **e, f** Flow cytometry analyses of CD86 and CD206 expression in BMDMs treated with PBS, MELR, HOCl-CDS, or HOCl-CDS hydrogel. **g** Cytotoxic effects of $RADA_{24}$ hydrogel, MELR hydrogel and HOCl-CDS hydrogel on B16–F10 cells. The data are presented as means ± SEM (n = 3).

tumor growth rate in MELR hydrogel-treated mice was similar to that of PBS-treated mice at later stages. HOCl-CDS also inhibited tumor growth, and HOCl-CDS hydrogel provided a stronger tumor-inhibitory effect than HOCl-CDS, especially at later stages of tumor progression (Fig. 4b and c). B16-LUC cells were inoculated to establish subcutaneous melanoma, and bioluminescence imaging was performed on days 8, 18, and 28 to monitor the tumor growth. Consistently, HOCl-CDS hydrogel provided the strongest inhibitory effect on tumor growth (Fig. 4d) and a superior ability to prolong the survival of tumor-bearing mice (Fig. 4e).

To investigate the biocompatibility of MELR hydrogel, HOCl-CDS, and HOCl-CDS hydrogel, blood and biochemical analyses were performed after subcutaneous injection. There was no significant weight decrease in any of the groups up to 3 weeks after treatment (Fig. 4f). The counts of RBCs, white blood cells (WBC), platelets (PLT), monocytes (Mon), and lymphocytes (Lymph), as well as the levels of gluTAMsic pyruvic transaminase (ALT), gluTAMsic oxaloacetic transaminase (AST), and blood urea nitrogen (BUN), were within physiological ranges and did not differ among the treatment groups (Fig. 4g and Fig. S6). These findings indicated that these treatments did not cause significant damage to the hematopoietic system, liver, and kidneys. Histological analyses confirmed that HOCl-CDS hydrogel did not cause pathological damage to the hearts, livers, spleens, lungs, and kidneys (Fig. 4h).

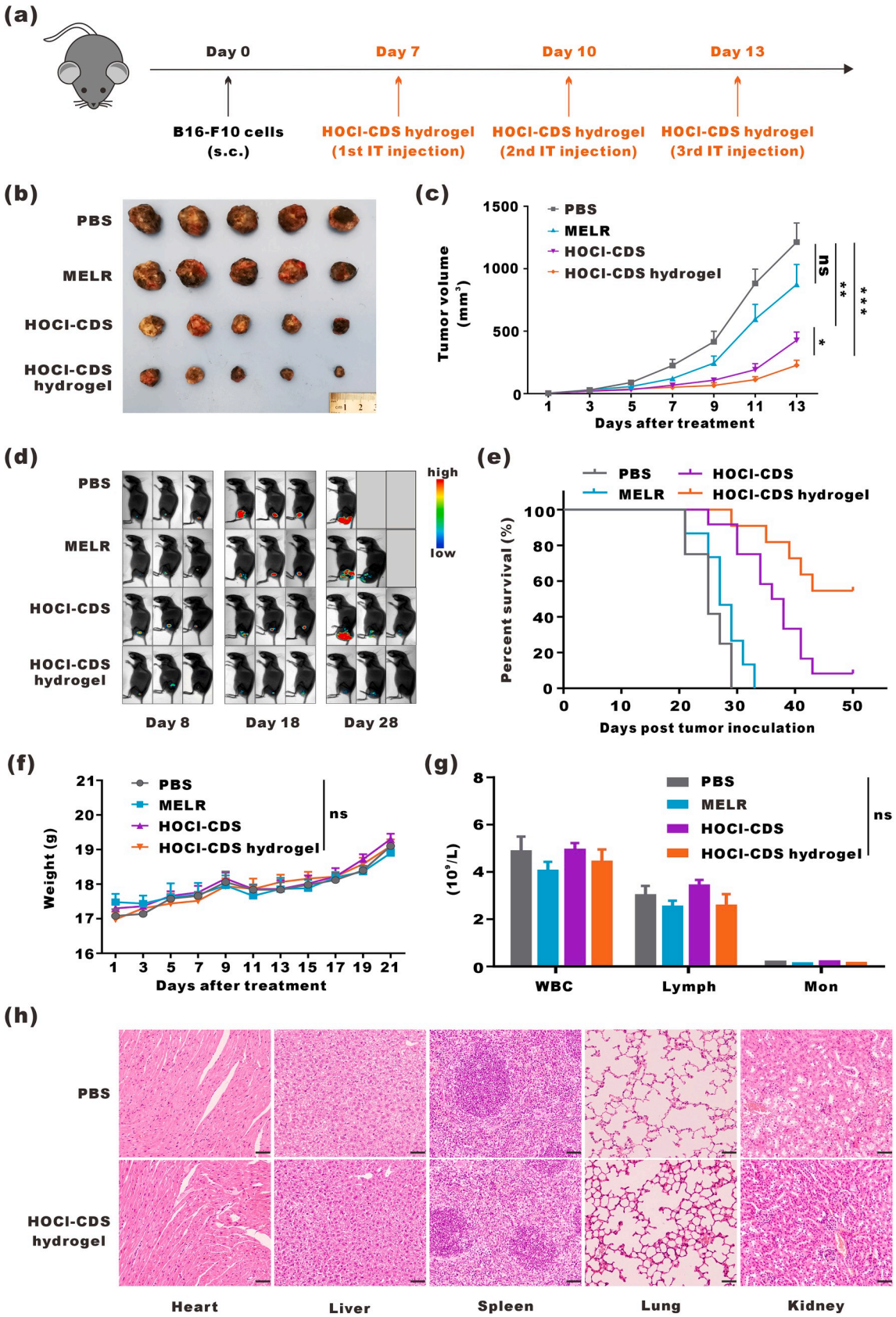

Fig. 4. *In vivo* antitumor effects of the HOCl-CDS hydrogel. **a** Schematic diagram of HOCl-CDS hydrogel treatment in mice bearing subcutaneous B16–F10 tumors. **b** Representative photographs of tumors. **c** Tumor growth curves. Data are presented as means ± SEM (n = 5–6). **d** Representative bioluminescence images of mice bearing B16-LUC tumors. **e** The survival curves of tumor-bearing mice (n = 12). **f** Weight of mice up to 21 d after treatment. Data are presented as means ± SEM (n = 7). **g** Hemanalysis on day 8 after treatment. Data are presented as means ± SEM (n = 5). **h** Micrographs of H&E staining of major organs; the scale bar indicates 50 μm.

3.5. *In vivo* immune activation by HOCl-CDS hydrogel

Next, the abilities of HOCl-CDS hydrogel to activate the immune system *in vivo* 8 d after intratumoral administration were explored (Fig. 5a). The proportion of mDCs in the lymph nodes of HOCl-CDS hydrogel-treated mice was 6.2-fold of that in PBS group (Fig. 5b). The proportion of tumor-infiltrating immune cells ($ZIR^{-}CD45^{+}$) in the HOCl-CDS hydrogel group was 19.1 %, 4.2-fold of that in the PBS group

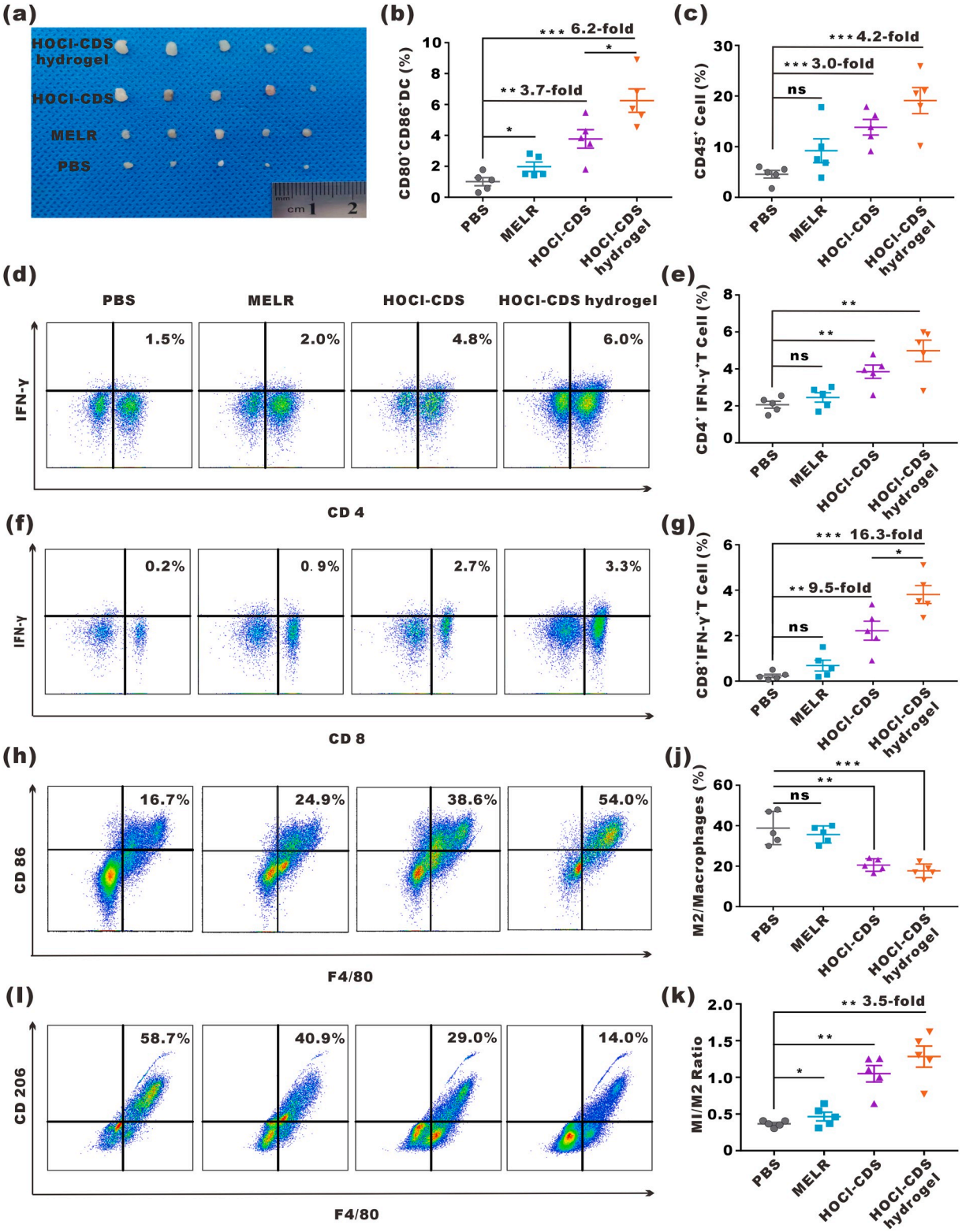

Fig. 5. *In vivo* immune cells activation by HOCl-CDS hydrogel. **a** Representative photographs of dissected inguinal lymph nodes. **b** Percentages of $CD80^{+}CD86^{+}$ DCs in inguinal lymph nodes. **c** Percentages of $CD45^{+}$ lymphocytes in the tumor microenvironment (TME). **d** Expression of CD4 and IFN-γ in T cells in the TME. **e** Percentages of $CD4^{+}IFN\gamma^{+}$ T cells in the TME. **f** Expression of CD8 and IFN-γ in T cells in the TME. **g** Percentages of $CD8^{+}IFN\gamma^{+}$ T cells in the TME. **h, i** Expression of CD86 and CD206 in TAMs in the TME. **j** Percentages of M2/total macrophages in the TME. **k** M1/M2 ratios. Data are presented as means ± SEM (n = 5).

(Fig. 5c). As type I helper T cells (Th1) and cytotoxic T lymphocytes (CTL) played an important role in antitumor immunity, we analyzed the ratio of $ZIR^-CD45^+CD3^+CD4^+IFN\text{-}\gamma^+$ cells (Th1) and $ZIR^-CD45^+CD3^+CD8^+IFN\text{-}\gamma^+$ cells (CTL) after treatments. As expected, treatment with HOCl-CDS hydrogel significantly enhanced the infiltration of CTLs and Th1 cells in the TME (Fig. 5d-g). To assess TAMs polarization, the expression of CD86 and CD206 were analyzed by flow cytometry. $ZIR^-CD11b^+F4/80^+CD86^+CD206^-$ cells represented M1-TAMs and $ZIR^-CD11b^+F4/80^+CD206^+CD86^-$ cells represented M2-TAMs. HOCl-CDS hydrogel group showed a reduced proportion of M2-TAMs and an increased proportion of M1-TAMs, and the ratio of M1/M2 was 3.5-fold of that in the PBS group, confirming that HOCl-CDS hydrogel promoted M1-TAMs polarization (Fig. 5h-k). These findings suggested that HOCl-CDS hydrogel promoted DC maturation, M1-TAMs polarization, and infiltration of Th1 cells and CTLs in the TME.

3.6. Antitumor effect of anti-PD-1 combined with HOCl-CDS hydrogel

HOCl-CDS hydrogel increased the expression levels of PD-L1 on both BMDCs and BMDMs (Fig. 6a and b). Further ELISA assay showed that compared to untreated-CDS group, HOCl-CDS group displayed higher level of secreted immunosuppressive cytokines, such as transforming growth factor-β1 (TGF-β1) and interleukin-6 (IL-6), which were reported to be related to the high expression of PD-L1 (Fig. S7). In addition, HOCl-CDS hydrogel promoted T cell infiltration and TME remodeling, which provided a rationale for PD-1 blockade combined with HOCl-CDS hydrogel treatment. We subcutaneously inoculated B16–F10 cells into C57BL/6J mice. When tumor volumes reached ~30 mm^3, mice were randomly divided into groups and treated with PBS, anti-PD-1 antibody (200 mg/kg, 4 times, every 2 d), HOCl-CDS hydrogel (3 times, every 3 d), and anti-PD-1 + HOCl-CDS hydrogel (Fig. 6c). The tumor growth and tumor weight until the volume of the PBS group reached 1000 mm^3 were recorded as Fig. 6d-f. Anti-PD-1 alone was insufficient to inhibit tumor growth, whereas the combination of anti-PD-1 with HOCl-CDS hydrogel dramatically inhibited tumor growth. The proportions of CTLs and Th1 cells in the tumors of mice treated with anti-PD-1 + HOCl-CDS hydrogel were 9.9 % and 6.4 %, respectively, which were 10.4-fold and 17.8-fold of that in the PBS group. Compared with anti-PD-1 or HOCl-CDS hydrogel alone, anti-PD-1 + HOCl-CDS hydrogel significantly increased the proportion of Th1 cells and CTLs. The ratio of $CD8^+/CD4^+$ T cells in the TME of combined group, associated with favorable prognosis after immunotherapy, also showed an increase compared to the anti-PD-1 alone, but not to the HOCl-CDS hydrogel alone (Fig. 6g-i).

4. Discussion

Although immunotherapies have changed melanoma treatment, not all patients respond [32–34]. More studies are trying to develop new strategies to potentiate cancer immunotherapy. In the cancer immunity cycle, DCs and macrophages play crucial roles in activating antitumor immune responses, linking innate and adaptive immunities. Antigens are captured by immature dendritic cells (imDCs), which are converted into mature dendritic cells (mDCs) expressing elevated levels of CD80 and CD86 and induce antigen-specific T cell responses. Macrophages are polarized into 2 distinct phenotypes in response to the surrounding microenvironment: M1 macrophages, which produce pro-inflammatory cytokines and cross-present antigens to $CD8^+$ T cells, or M2 macrophages, which produce anti-inflammatory cytokines to inhibit adaptive immunity and promote tumor progression. In this study, we compared immunostimulatory effects of hypoxia, DDP, RAD, PDT and HOCl treated-CDS on DCs maturation and macrophages polarization, and found that HOCl-treated tumor CDS (HOCl-CDS) exhibited the strongest immunostimulatory effects. Therefore, we developed a new immunotherapeutic strategy based on HOCl-CDS.

HOCl is an oxidant that has been demonstrated to participate in immunogenic modulation, and it can increase the immunogenicity of antigens through oxidation modifications, that increase recognition, capture and processing by APCs [34–40]. Chiang et al. showed that compared to the traditional methods, such as freeze-thaw cycles and UVB-irradiation to treat tumor cells, HOCl-oxidation induces rapid primary necrotic tumor cell death, protein oxidation, and increased expression of chaperones and antioxidant proteins, leading to activation of oxidative stress-response pathways [41]. Treatment of ovarian epithelial cancer cells (SKOV-3) with HOCl can enhance antigens immunogenicity allowing for improved tumor antigen processing and presentation by DCs, resulting in production of Th1-priming cytokines and chemokines and stimulation of robust tumor-specific IFN-γ secretions in autologous T-cells [42,43]. On the other hand, tumor cells frequently produce suppressive molecules after exogenous treatments that could inhibit DC activation, including prostaglandin E2(PGE2). Treatment of HOCl-oxidation but not others might inactivate these suppressive molecules, leading to improved DC maturation [44]. In this study, HOCl-CDS were generated by treating B16–F10 cells with HOCl to induce immune stimulation. Through the detection and analysis of the contents in HOCl-CDS, we found that HOCl-CDS contained high-levels of cytokines and chemokines related to DC maturation and macrophage polarization, including TNF- α, IL-1α, GM-CSF, M-CSF, MIP-3α, MIP-1α, ENA78, CD40L, MCP1, HMGB1 and ATP, a decreased immunosuppressive molecule level of PGE2 compared with DDP treatment.

We also developed a MELR hydrogel, which directly killed tumor cells and prolonged the retention of HOCl-CDS in the TME. MELR hydrogel was composed of melittin, linker peptides, and the synthetic polypeptide $RADA_{24}$. Melittin, which is composed of 26 amino acids with α-helical conformation, including a hydrophobic amino-terminal region and a hydrophilic carboxy-terminal region, is the main component of bee venom and has strong cytotoxic effects on tumor cells [45,46]. The synthetic peptide $RADA_{24}$ is composed of 4 amino acids (Arg-Ala-Asp-Ala, RADA) repeated 6 times. $RADA_{24}$ self-assembles into hydrogel with nanofiber structure, reducing the hemolytic effects of melittin. The α-helical conformation of melittin makes it possible to be linked to the polypeptide $RADA_{24}$ by physical cross-linking methods to form cross-linked nanofibers MELR [47]. Studies have shown that melittin can increase the secretion of immunostimulatory cytokines including IL-2, INF-γ, TNF-α, and promote the activation of cytotoxic T cells and natural killer cells. However, its hemolysis and toxicity limit the application. Direct injection of melittin solutions may lead to toxic effects [30]. Therefore, the physical cross-linking strategy between $RADA_{24}$ and melittin to form MELR hydrogel can not only alleviate the toxicity, but also cooperate with HOCl-CDS to exert immunostimulatory effect. Herein, MELR was shown to be a suitable delivery platform, in addition to eliminating tumor cells directly and exhibiting the synergistic effect of immune activation.

Multifunctional HOCl-CDS hydrogel was developed by loading HOCl-CDS to MELR hydrogel, and provided the following advantages: (1) Robust immunostimulation ability, stronger than that of traditional methods. Notably, HOCl-CDS hydrogel promoted DC maturation, M1-TAMs polarization, and effector T cell activation. These effects remodeled the TME. (2) Direct killing effects. MELR exerted cytotoxic effects on tumor cells, and the addition of HOCl-CDS did not impair the ability. The direct killing effect of HOCl-CDS hydrogel reduced tumor growth, providing more time for immune cells to inhibit cancer progression. (3) Sustained cargo release. MELR hydrogel allowed for a sustained HOCl-CDS release at the tumor site. The constant immunostimulatory effect of the formulation enhanced therapeutic effects of anti-cancer interventions. (4) Excellent biocompatibility. HOCl-CDS hydrogel did not cause significant side effects in mice, displaying great potential for clinical translation. (5) Multiple therapeutic targets. HOCl-CDS hydrogel targeted both tumor cells and immune cells involved in the cancer immunity cycle [7]. Additionally, HOCl-CDS hydrogels increased the expression of PD-L1 on DCs and macrophages. PD-L1, the ligand of PD-1 expressed on the surface of activated T cells, promotes T cell exhaustion, hampering antitumor T cell responses. Anti-PD-1 treatment inhibits the

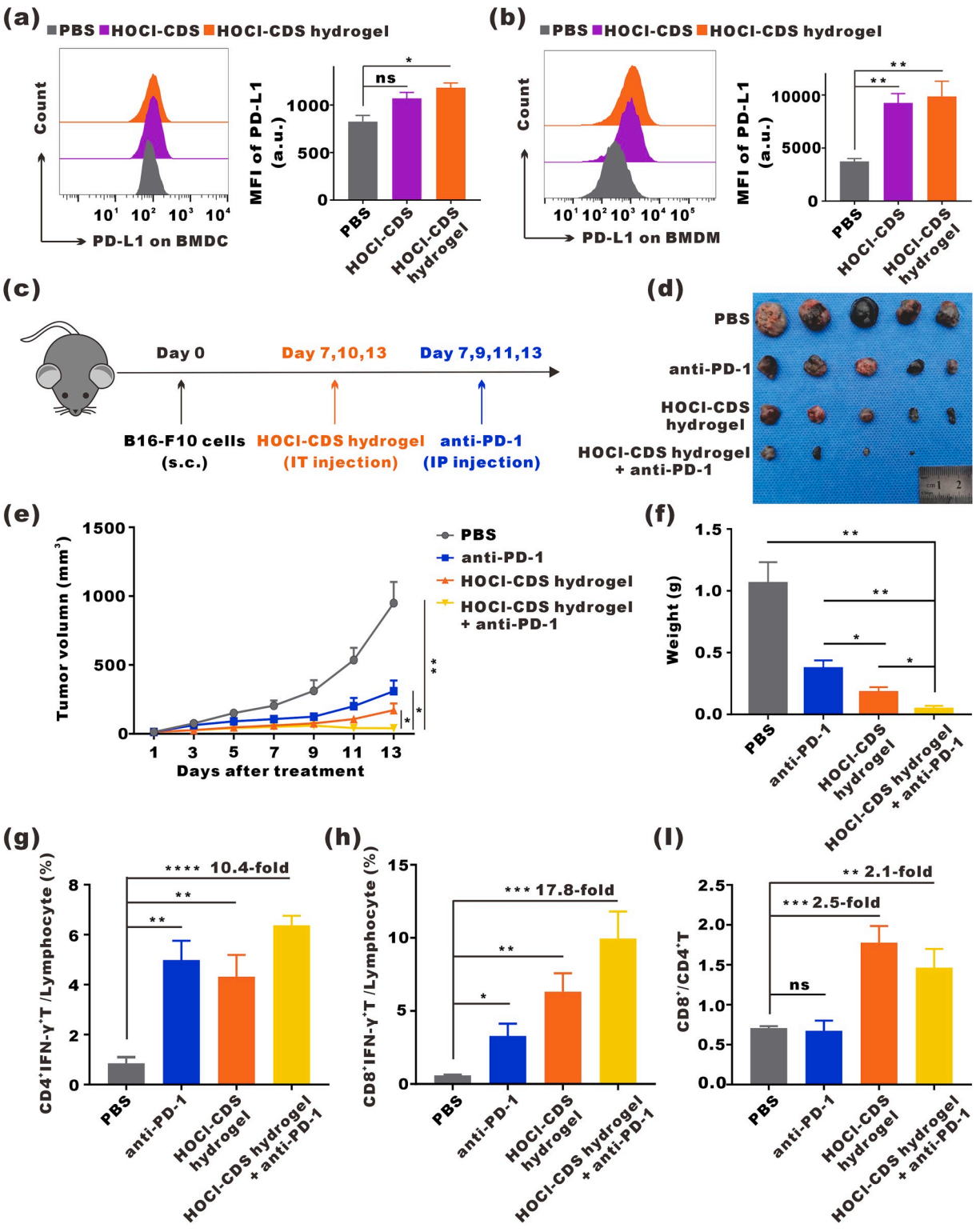

Fig. 6. Antitumor effects of anti-PD-1 combined with HOCl-CDS hydrogel. **a** Expression of PD-L1 on BMDCs treated with PBS, HOCl-CDS, or HOCl-CDS hydrogel. Data are presented as means ± SEM (n = 3). **b** Expression of PD-L1 on BMDMs stimulated with PBS, HOCl-CDS, or HOCl-CDS hydrogel. Data are presented as means ± SEM (n = 3). **c** Schematic diagram of HOCl-CDS hydrogel treatment combined with anti-PD-1 treatment in mice bearing subcutaneous B16–F10 tumors. **d** Representative photographs of tumors dissected from mice subcutaneously injected with B16–F10. **e** Tumor growth curves. Data are presented as means ± SEM (n = 5). **f** Weight of the dissected tumors. Data are presented as means ± SEM (n = 4–5). **g** Percentages of $CD4^+IFN\gamma^+$ T cells in the tumor microenvironment. **h** Percentages of $CD8^+IFN\gamma^+$ T cells in the tumor microenvironment. **i** $CD8^+/CD4^+$ T cell ratios. Data are presented as means ± SEM (n = 4–5).

PD-1/PD-L1 pathway and restores effector T cell function [48]. The remodeling effect on the TME of HOCl-CDS hydrogel also promoted the efficacy of anti-PD-1 therapies. We found that the combination of HOCl-CDS hydrogel with anti-PD-1 treatment was more effective in tumor inhibition than HOCl-CDS hydrogel or PD-1 blockade alone. Therefore, HOCl-CDS hydrogel not only provides a promising new strategy to increase immune response in melanoma but also provides a new direction for the development of combination immunotherapeutic approaches. For patients with unresectable or advanced melanoma, HOCl-CDS hydrogel can be injected into several lesions combined with anti-PD-1 agents simultaneously or sequentially, potentially leading to durable tumor control. The CDS can also be genetically engineered to express immunostimulatory cytokines to further increase its therapeutic potential.

5. Conclusions

Immunotherapy resistance remains a significant clinical challenge. In this study, we developed a multifunctional HOCl-CDS hydrogel by loading the strongly immunogenic HOCl-CDS into a MELR hydrogel. HOCl-CDS hydrogel showed potent antitumor efficacy in melanoma by inducing direct tumor cell death and remodeling the TME. Furthermore, the HOCl-CDS hydrogel augmented the antitumor effects of anti-PD-1 treatment in the syngeneic melanoma mouse model, suggesting that HOCl-CDS hydrogel is a promising immunotherapeutic approach for local tumor treatments.

CRediT authorship contribution statement

Yuhan Zhou: Investigation, Methodology, Writing – original draft. **Ting Ye:** Data curation, Validation, Writing – original draft. **Chengzhi Ye:** Investigation, Formal analysis, Writing – review & editing. **Chao Wan:** Investigation. **Siyue Yuan:** Investigation. **Yushuai Liu:** Investigation. **Tianyu Li:** Investigation. **Fagang Jiang:** Funding acquisition. **Jonathan F. Lovell:** Methodology, Resources. **Honglin Jin:** Conceptualization, Methodology, Supervision, Resources, Funding acquisition. **Jing Chen:** Conceptualization, Methodology, Supervision, Resources, Funding acquisition.

Declaration of competing interest

The authors declare that they have no known competing financial interests or personal relationships that could have appeared to influence the work reported in this paper.

Acknowledgements

This work was supported by the National Natural Science Foundation of China (No. 81773285, 81874233 and 82022040), Health Commission of Hubei Province scientific research project (WJ2021Z004), Scientific Research Project of Hubei Provincial Health and Family Planning Commission, China (WJ2015MB017 to J.C.).

Appendix A. Supplementary data

Supplementary data to this article can be found online at https://doi.org/10.1016/j.bioactmat.2021.07.019.

References

[1] U. Sahin, Ö. Türeci, Personalized vaccines for cancer immunotherapy, Science (New York, NY) 359 (2018) 1355–1360, https://doi.org/10.1126/science.aar7112.

[2] B. Sun, H. Hyun, L.T. Li, A.Z. Wang, Harnessing nanomedicine to overcome the immunosuppressive tumor microenvironment, Acta Pharmacol. Sin. 41 (2020) 970–985, https://doi.org/10.1038/s41401-020-0424-4.

[3] M.M. Gubin, X. Zhang, H. Schuster, E. Caron, J.P. Ward, T. Noguchi, Y. Ivanova, J. Hundal, C.D. Arthur, W.J. Krebber, G.E. Mulder, M. Toebes, M.D. Vesely, S. S. Lam, A.J. Korman, J.P. Allison, G.J. Freeman, A.H. Sharpe, E.L. Pearce, T. N. Schumacher, R. Aebersold, H.G. Rammensee, C.J. Melief, E.R. Mardis, W. E. Gillanders, M.N. Artyomov, R.D. Schreiber, Checkpoint blockade cancer immunotherapy targets tumour-specific mutant antigens, Nature 515 (2014) 577–581, https://doi.org/10.1038/nature13988.

[4] L. Hirsch, L. Zitvogel, A. Eggermont, A. Marabelle, PD-Loma: a cancer entity with a shared sensitivity to the PD-1/PD-L1 pathway blockade, Br. J. Canc. 120 (2019) 3–5, https://doi.org/10.1038/s41416-018-0294-4.

[5] D.H. Peng, B.L. Rodriguez, L. Diao, Collagen promotes anti-PD-1/PD-L1 resistance in cancer through LAIR1-dependent CD8(+) T cell exhaustion, 11, 2020, p. 4520, https://doi.org/10.1038/s41467-020-18298-8.

[6] J.A. Joyce, D.T. Fearon, T cell exclusion, immune privilege, and the tumor microenvironment, Science (New York, NY) 348 (2015) 74–80, https://doi.org/10.1126/science.aaa6204.

[7] D.S. Chen, I. Mellman, Oncology meets immunology: the cancer-immunity cycle, Immunity 39 (2013) 1–10, https://doi.org/10.1016/j.immuni.2013.07.012.

[8] A. MartIn-Fontecha, S. Sebastiani, U.E. Höpken, M. Uguccioni, M. Lipp, A. Lanzavecchia, F. Sallusto, Regulation of dendritic cell migration to the draining lymph node: impact on T lymphocyte traffic and priming, J. Exp. Med. 198 (2003) 615–621, https://doi.org/10.1084/jem.20030448.

[9] K. Hildner, B.T. Edelson, W.E. Purtha, M. Diamond, H. Matsushita, M. Kohyama, B. Calderon, B.U. Schraml, E.R. Unanue, M.S. Diamond, R.D. Schreiber, T. L. Murphy, K.M. Murphy, Batf3 deficiency reveals a critical role for CD8alpha+ dendritic cells in cytotoxic T cell immunity, Science (New York, NY) 322 (2008) 1097–1100, https://doi.org/10.1126/science.1164206.

[10] C.S. Garris, S.P. Arlauckas, R.H. Kohler, M.P. Trefny, S. Garren, C. Piot, C. Engblom, C. Pfirschke, M. Siwicki, J. Gungabeesoon, G.J. Freeman, S.E. Warren, S. Ong, E. Browning, C.G. Twitty, R.H. Pierce, M.H. Le, A.P. Algazi, A.I. Daud, S. I. Pai, A. Zippelius, R. Weissleder, M.J. Pittet, Successful anti-PD-1 cancer immunotherapy requires T cell-dendritic cell crosstalk involving the cytokines IFN-γ and IL-12, Immunity 49 (2018) 1148–1161, https://doi.org/10.1016/j.immuni.2018.09.024, e7.

[11] E. Peranzoni, J. Lemoine, L. Vimeux, V. Feuillet, S. Barrin, C. Kantari-Mimoun, N. Bercovici, M. Guérin, J. Biton, H. Ouakrim, F. Régnier, A. Lupo, M. Alifano, D. Damotte, E. Donnadieu, Macrophages impede CD8 T cells from reaching tumor cells and limit the efficacy of anti-PD-1 treatment, Proceedings of the National Academy of Sciences of the United States of America 115 (2018), https://doi.org/10.1073/pnas.1720948115. E4041-e50.

[12] L. Cassetta, J.W. Pollard, Targeting macrophages: therapeutic approaches in cancer, Nat. Rev. Drug Discov. 17 (2018) 887–904, https://doi.org/10.1038/nrd.2018.169.

[13] J. Cai, Q. Qi, X. Qian, J. Han, X. Zhu, Q. Zhang, R. Xia, The role of PD-1/PD-L1 axis and macrophage in the progression and treatment of cancer, J. Canc. Res. Clin. Oncol. 145 (2019) 1377–1385, https://doi.org/10.1007/s00432-019-02879-2.

[14] S.P. Arlauckas, C.S. Garris, In vivo imaging reveals a tumor-associated macrophage-mediated resistance pathway in anti-PD-1 therapy, 9, 2017, https://doi.org/10.1126/scitranslmed.aal3604.

[15] A. Mantovani, F. Marchesi, A. Malesci, L. Laghi, P. Allavena, Tumour-associated macrophages as treatment targets in oncology, Nat. Rev. Clin. Oncol. 14 (2017) 399–416, https://doi.org/10.1038/nrclinonc.2016.217.

[16] D.C. Hinshaw, L.A. Shevde, The tumor microenvironment innately modulates cancer progression, Canc. Res. 79 (2019) 4557–4566, https://doi.org/10.1158/0008-5472.can-18-3962.

[17] M. Dougan, S.K. Dougan, Targeting immunotherapy to the tumor microenvironment, 118, 2017, pp. 3049–3054, https://doi.org/10.1002/jcb.26005.

[18] J. Wolfers, A. Lozier, G. Raposo, A. Regnault, C. Théry, C. Masurier, C. Flament, S. Pouzieux, F. Faure, T. Tursz, E. Angevin, S. Amigorena, L. Zitvogel, Tumor-derived exosomes are a source of shared tumor rejection antigens for CTL cross-priming, Nat. Med. 7 (2001) 297–303, https://doi.org/10.1038/85438.

[19] B. Escudier, T. Dorval, N. Chaput, F. André, M.P. Caby, S. Novault, C. Flament, C. Leboulaire, C. Borg, S. Amigorena, C. Boccaccio, C. Bonnerot, O. Dhellin, M. Movassagh, S. Piperno, C. Robert, V. Serra, N. Valente, J.B. Le Pecq, A. Spatz, O. Lantz, T. Tursz, E. Angevin, L. Zitvogel, Vaccination of metastatic melanoma patients with autologous dendritic cell (DC) derived-exosomes: results of thefirst phase I clinical trial, J. Transl. Med. 3 (2005) 10, https://doi.org/10.1186/1479-5876-3-10.

[20] Z. Yin, J. Fan, J. Xu, F. Wu, Y. Li, M. Zhou, T. Liao, L. Duan, S. Wang, W. Geng, Y. Jin, Z. Yin, J. Fan, J. Xu, F. Wu, Y. Li, M. Zhou, T. Liao, L. Duan, S. Wang, W. Geng, Y. Jin, Immunoregulatory roles of extracellular vesicles and associated therapeutic applications in lung cancer, Front. Immunol. 11 (2020) 2024, https://doi.org/10.3389/fimmu.2020.02024.

[21] Y. Ning, K. Shen, Q. Wu, X. Sun, Y. Bai, Y. Xie, J. Pan, C. Qi, Tumor exosomes block dendritic cells maturation to decrease the T cell immune response, Immunol. Lett. 199 (2018) 36–43, https://doi.org/10.1016/j.imlet.2018.05.002.

[22] H. Zhang, K. Tang, Y. Zhang, R. Ma, J. Ma, Y. Li, S. Luo, X. Liang, T. Ji, Z. Gu, J. Lu, W. He, X. Cao, Y. Wan, B. Huang, Cell-free tumor microparticle vaccines stimulate dendritic cells via cGAS/STING signaling, Cancer immunology research 3 (2015) 196–205, https://doi.org/10.1158/2326-6066.cir-14-0177.

[23] C. Wan, Y. Sun, Y. Tian, L. Lu, X. Dai, J. Meng, J. Huang, Q. He, B. Wu, Z. Zhang, K. Jiang, D. Hu, G. Wu, J.F. Lovell, H. Jin, K. Yang, Irradiated tumor cell-derived microparticles mediate tumor eradication via cell killing and immune reprogramming, 6, 2020, eaay9789, https://doi.org/10.1126/sciadv.aay9789.

[24] T. Chen, J. Guo, M. Yang, X. Zhu, X. Cao, Chemokine-containing exosomes are released from heat-stressed tumor cells via lipid raft-dependent pathway and act as efficient tumor vaccine, J. Immunol. 186 (2011) 2219–2228, https://doi.org/10.4049/jimmunol.1002991.
[25] M. Guo, F. Wu, Autologous Tumor Cell-Derived Microparticle-Based Targeted Chemotherapy in Lung Cancer Patients with Malignant Pleural Effusion, 11, 2019, https://doi.org/10.1126/scitranslmed.aat5690.
[26] R. Ma, T. Ji, D. Chen, W. Dong, H. Zhang, X. Yin, J. Ma, X. Liang, Y. Zhang, G. Shen, X. Qin, B. Huang, Tumor cell-derived microparticles polarize M2 tumor-associated macrophages for tumor progression, OncoImmunology 5 (2016), e1118599, https://doi.org/10.1080/2162402x.2015.1118599.
[27] J. Chen, W. Sun, H. Zhang, J. Ma, P. Xu, Y. Yu, H. Fang, L. Zhou, J. Lv, J. Xie, Y. Liu, K. Tang, B. Huang, Macrophages reprogrammed by lung cancer microparticles promote tumor development via release of IL-1β, Cell. Mol. Immunol. (2019) https://doi.org/10.1038/s41423-019-0313-2.
[28] M. Chen, Y. Tan, Z. Dong, J. Lu, X. Han, Q. Jin, W. Zhu, J. Shen, L. Cheng, Injectable Anti-inflammatory nanofiber hydrogel to achieve systemic immunotherapy post local administration, 20, 2020, pp. 6763–6773, https://doi.org/10.1021/acs.nanolett.0c02684.
[29] Y. Li, Z. Su, W. Zhao, X. Zhang, N. Momin, C. Zhang, K.D. Wittrup, Y. Dong, D. J. Irvine, R. Weiss, Multifunctional oncolytic nanoparticles deliver self-replicating IL-12 RNA to eliminate established tumors and prime systemic immunity, Nature Cancer 1 (2020) 882–893, https://doi.org/10.1038/s43018-020-0095-6.
[30] J. Zhou, C. Wan, J. Cheng, H. Huang, J.F. Lovell, Delivery strategies for melittin-based cancer therapy, 13, 2021, pp. 17158–17173, https://doi.org/10.1021/acsami.1c03640.
[31] H. Jin, C. Wan, Z. Zou, Tumor ablation and therapeutic immunity induction by an injectable peptide hydrogel, 12, 2018, pp. 3295–3310, https://doi.org/10.1021/acsnano.7b08148.
[32] A. Ribas, J.D. Wolchok, Cancer immunotherapy using checkpoint blockade, 359, 2018, pp. 1350–1355, https://doi.org/10.1126/science.aar4060.
[33] P. Sharma, J.P. Allison, The future of immune checkpoint therapy, Science (New York, NY) 348 (2015) 56–61, https://doi.org/10.1126/science.aaa8172.
[34] J. Marcinkiewicz, B.M. Chain, E. Olszowska, S. Olszowski, J.M. Zgliczyński, Enhancement of immunogenic properties of ovalbumin as a result of its chlorination, Int. J. Biochem. 23 (1991) 1393–1395, https://doi.org/10.1016/0020-711x(91)90280-z.
[35] J. Marcinkiewicz, E. Olszowska, S. Olszowski, J.M. Zgliczynski, Enhancement of trinitrophenyl-specific humoral response to TNP proteins as the result of carrier chlorination, Immunology 76 (1992) 385–388.
[36] M.E. Allison, D.T. Fearon, Enhanced immunogenicity of aldehyde-bearing antigens: a possible link between innate and adaptive immunity, Eur. J. Immunol. 30 (2000) 2881–2887, https://doi.org/10.1002/1521-4141(200010)30:10<2881::aid-immu2881>3.0.co;2-9.
[37] M.K. Callahan, D. Chaillot, C. Jacquin, P.R. Clark, A. Ménoret, Differential acquisition of antigenic peptides by Hsp70 and Hsc70 under oxidative conditions, J. Biol. Chem. 277 (2002) 33604–33609, https://doi.org/10.1074/jbc.M202890200.
[38] R. Zhou, W.J. Huang, C. Ma, Y. Zhou, Y.Q. Yao, Y.X. Wang, L.T. Gou, C. Yi, J. L. Yang, HOCl oxidation-modified CT26 cell vaccine inhibits colon tumor growth in a mouse model, Asian Pac. J. Cancer Prev. APJCP : APJCP. 13 (2012) 4037–4043, https://doi.org/10.7314/apjcp.2012.13.8.4037.
[39] M. Reth, Hydrogen peroxide as second messenger in lymphocyte activation, Nat. Immunol. 3 (2002) 1129–1134, https://doi.org/10.1038/ni1202-1129.
[40] G. Bauer, HOCl and the control of oncogenesis, J. Inorg. Biochem. 179 (2018) 10–23, https://doi.org/10.1016/j.jinorgbio.2017.11.005.
[41] M. Graciotti, F. Marino, H. Pak, P. Baumgaertner, A.C. Thierry, J. Chiffelle, M.A. S. Perez, Deciphering the Mechanisms of Improved Immunogenicity of Hypochlorous Acid-Treated Antigens in Anti-cancer Dendritic Cell-Based Vaccines, 8, 2020, https://doi.org/10.3390/vaccines8020271.
[42] C.L. Chiang, J.A. Ledermann, A.N. Rad, D.R. Katz, B.M. Chain, Hypochlorous acid enhances immunogenicity and uptake of allogeneic ovarian tumor cells by dendritic cells to cross-prime tumor-specific T cells. Cancer immunology, immunotherapy, CII 55 (2006) 1384–1395, https://doi.org/10.1007/s00262-006-0127-9.
[43] C.L. Chiang, J.A. Ledermann, E. Aitkens, E. Benjamin, D.R. Katz, B.M. Chain, Oxidation of ovarian epithelial cancer cells by hypochlorous acid enhances immunogenicity and stimulates T cells that recognize autologous primary tumor, Clin. Canc. Res. : an official journal of the American Association for Cancer Research 14 (2008) 4898–4907, https://doi.org/10.1158/1078-0432.CCR-07-4899.
[44] C.L. Chiang, L.E. Kandalaft, J. Tanyi, A.R. Hagemann, G.T. Motz, N. Svoronos, K. Montone, G.M. Mantia-Smaldone, L. Smith, H.L. Nisenbaum, B.L. Levine, M. Kalos, B.J. Czerniecki, D.A. Torigian, D.J. Powell Jr., R. Mick, G. Coukos, A dendritic cell vaccine pulsed with autologous hypochlorous acid-oxidized ovarian cancer lysate primes effective broad antitumor immunity: from bench to bedside, Clin. Canc. Res. : an official journal of the American Association for Cancer Research 19 (2013) 4801–4815, https://doi.org/10.1158/1078-0432.ccr-13-1185.
[45] H. Memariani, M. Memariani, Melittin: from honeybees to superbugs, 103, 2019, pp. 3265–3276, https://doi.org/10.1007/s00253-019-09698-y.
[46] H. Jin, G. Zhao, J. Hu, Q. Ren, K. Yang, C. Wan, A. Huang, P. Li, J.P. Feng, J. Chen, Z. Zou, Melittin-containing hybrid peptide hydrogels for enhanced photothermal therapy of glioblastoma, ACS Appl. Mater. Interfaces 9 (2017) 25755–25766, https://doi.org/10.1021/acsami.7b06431.
[47] X. Dai, J. Meng, S. Deng, L. Zhang, C. Wan, L. Lu, J. Huang, Y. Hu, Z. Zhang, Y. Li, J.F. Lovell, G. Wu, K. Yang, H. Jin, Targeting CAMKII to reprogram tumor-associated macrophages and inhibit tumor cells for cancer immunotherapy with an injectable hybrid peptide hydrogel, Theranostics 10 (2020) 3049–3063, https://doi.org/10.7150/thno.42385.
[48] J. Gong, A. Chehrazi-Raffle, S. Reddi, R. Salgia, Development of PD-1 and PD-L1 Inhibitors as a Form of Cancer Immunotherapy: a Comprehensive Review of Registration Trials and Future Considerations, 6, 2018, p. 8, https://doi.org/10.1186/s40425-018-0316-z.